

Cite this: DOI: 00.0000/xxxxxxxxxx

Effect of ring stiffness and ambient pressure on the dynamical slowdown in ring polymers †

Projesh Kumar Roy,^{a,b} Pinaki Chaudhuri,^{a,b,*} and Satyavani Vemparala^{a,b,*}Received Date
Accepted Date

DOI: 00.0000/xxxxxxxxxx

Using extensive molecular dynamics simulations, we investigate the slowing down of dynamics in a 3D system of ring polymers by varying the ambient pressure and the stiffness of the rings. Our study demonstrates that the stiffness of the rings determines the dynamics of the ring polymers, leading to glassiness at lower pressures for stiffer rings. The threading of the ring polymers, a unique feature that emerges only due to the topological nature of such polymers in three dimensions, is shown to be the determinant feature of dynamical slowing down, albeit only at a certain stiffness range. Our results suggest a possible framework of exploring the phase space spanned by ring stiffness and pressure to obtain spontaneously emerging topologically constrained polymer glasses, showing that it is not required to have pinning constructions to generate these glassy states.

1 Introduction

Entanglement in dense polymeric systems can arise due to many reasons and can lead to interesting and complex rheological phenomena. For linear polymer melt systems, entanglement can arise from spatial confinement via the presence of other linear polymers in close contact. It is intuitive that behavior of a single polymer in dilute vs dense melt conditions is very different. In the former case, the dynamics that govern the polymer behavior are largely determined by the interconnectivity of the polymer and the nature of the solvent surrounding it, while in the latter, the presence of other polymer molecules within close vicinity can significantly influence the dynamics of the polymers. Theoretical models exist to describe these two different scenarios: Rouse-Zimm model^{1–4} for extreme dilute systems, reptation or tube models^{5–8} for the dense linear polymer melt systems.

Entanglement can also arise from topological constraints via connecting the ends of the linear polymers resulting in ring polymers and consequently exhibiting different rheological properties^{9–19}. The ring polymers have been considered as model systems for understanding the compaction and organization of biologically relevant polymers like chromatin^{20–23}. In addition, recent studies^{24–27} have shown that systems composed of deformable particles such as colloids exhibit glassy behavior as a function of packing fraction. The introduction of deformability

and softness in the particles can induce novel packing behaviour at high densities, which is not possible to realize via spherical particles. The ring polymer systems thus can be an excellent model platform to mimic such colloids, with the possibility of soft and tuneable interactions, to understand emergence of glassy behavior in such colloidal systems. The complex behavior of the dynamics of the ring polymers poses an interesting challenge to the theoretical understanding of polymer entanglement. In the last decade, several attempts were made to understand their dynamical as well as statistical properties using computer simulations^{10–12}. Ring polymers show a sluggish zero-shear stress relaxation modulus (G) at longer time-scales when compared with theoretical models for such polymers^{28–30}. It was postulated that such deviation is caused by ring-ring penetration, or *threading* effect, which was not incorporated in the theoretical models like self-similar lattice-animal model^{31,32} annealed-tree model^{33,34}, or fractal loopy globule model³⁵. Despite pure linear polymer melts not exhibiting similar dynamical behavior, it was shown that the presence of even a small amount of linear polymers in the ring polymer melt can dramatically increase the relaxation times and make the ring polymer melt more sluggish^{21,28,36–39}. Assuming a similarity of the conformations between the ring and linear polymers at a length scale smaller than the radius of gyration (R_g), some modified theories have been proposed to incorporate the threading effect in pure ring polymer melts, e.g. Tsalikis *et al*³⁰, Dell *et al*⁴⁰.

Recently, it was shown that the dynamics of the ring polymer melts mimics a glassy behavior when a randomly chosen minute fraction of the rings are pinned in the simulation box^{41–43}. Further, it was estimated that at a large chain-length of ~ 3500 , glass formation of the ring polymer melts becomes spontaneous and independent of any external perturbations like pinning⁴¹. This

^a The Institute of Mathematical Sciences, C.I.T. Campus, Taramani, Chennai 600113, India; Tel: +914422543293/+914422543257; E-mail: pinakic@imsc.res.in/vani@imsc.res.in

^b Homi Bhabha National Institute, Training School Complex, Anushakti Nagar, Mumbai 400094, India

† Electronic Supplementary Information (ESI) available: See DOI: 10.1039/cXsm00000x/

type of glass formation is unique as it does not require any cooling, jamming, or modification of the interaction energies⁴⁴. Such glass-forming systems are termed *topological-glass*⁴⁵ which linear polymers fail to exhibit⁴⁶. The phenomenon of topological glass formation as well as the slow relaxation of G, was explained using the threading effect. This theory suggests that the glassy phase originates as a result of the long-range entanglements of the ring polymers in the form of threading, which creates insurmountable energetic barriers for the reptation movement of the ring polymers at larger timescale^{31,32}. Formation of such barriers is controlled by the topology (or conformations) and entropically driven mixing of the rings. Several studies have been performed to understand the effect of threading on the dynamics of the pure ring polymer melts without any external perturbations using Monte-Carlo (MC)^{18,45} and Molecular-Dynamics (MD)^{30,46–49} methods and by experiments^{50–52}.

In this paper, we focus on emergence of dynamical slowing down in systems of equilibrated ring polymer melts and identify the domain in phase space spanned by pressure and ring stiffness, i.e. $(P-K_\theta)$, where the glassy regime would be obtained as evidenced via our observations of increasingly slow dynamics within the ring polymer melt. Importantly, we observe that stiffer ring polymers exhibit dynamical slowdown at smaller ambient pressures. We explicitly calculate the total effect of threading in the melt configuration, and show that threading effect is directly contributing to the observed slowdown at certain $P-K_\theta$ state points. The pressure induced conformational changes of the ring polymers and their effects on the threading properties in equilibrium are also discussed.

The paper is organized as follows. After this introductory section, we provide a section on methods where the model system that we study and the details of the simulations that we perform are outlined. Subsequently, there is an extensive section discussing our results, where we detail the dynamical and structural properties of the system, and the correlations between the two. Finally, we have a concluding section where we summarize our findings and provide some future perspectives.

2 Methods

2.1 Simulation details

A series of molecular dynamics (MD) simulations of ring polymer melts are performed to analyze the slowing down in dynamical behavior of the systems with different values of ring stiffness and applied pressure. The pairwise potential of the ring polymers is modeled using the Kremer-Grest (KG) model^{11,12,53}. In KG model, the repulsive part of a truncated and shifted Lennard-Jones potential, aka Weeks-Chandler-Anderson (WCA) potential⁵⁴, is used to model the monomer-monomer non-bonded interactions;

$$U_{pair}(r_{ij}) = \begin{cases} 4\epsilon \left[\left(\frac{\sigma}{r_{ij}} \right)^{12} - \left(\frac{\sigma}{r_{ij}} \right)^6 + \frac{1}{4} \right] & r_{ij} \leq 2^{1/6} \\ 0 & r_{ij} > 2^{1/6} \end{cases} \quad (1)$$

where σ and ϵ are length and energy scales, respectively. ϵ is measured in $k_B T$ units, where k_B is the Boltzmann constant,

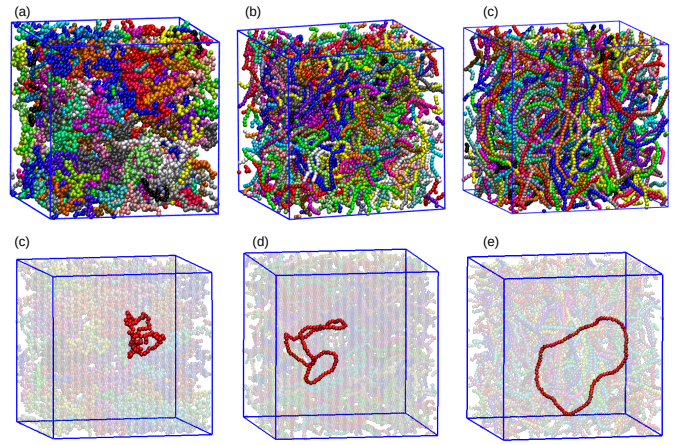


Fig. 1 (Top) Snapshots of the bulk phase at $P=0.010$ and $K_\theta=1$ (a), 10 (b), and 20 (c) at the end of equilibration runs. (Bottom) Conformation of a single polymer inside the bulk at these P and K_θ values in (c), (d), and (e).

and T is the temperature. A finitely extensible non-linear elastic (FENE) potential⁵³ is used to define the covalent bonds between the monomers:

$$U_{FENE}(r_{ij}) = \begin{cases} -0.5\kappa R_0^2 \ln \left[1 - \left(\frac{r_{ij}}{R_0} \right)^2 \right] & r_{ij} < R_0 \\ \infty & r_{ij} \geq R_0 \end{cases} \quad (2)$$

where $\kappa = 30$, $R_0 = 1.5$. In our paper, we have used the Kratky-Porod model⁵⁵, recently used in reference 49, for controlling the ring stiffness,

$$U_{angle}(\theta_i) = K_\theta [1 - \cos(\theta_i - \pi)] \quad (3)$$

where K_θ is the stiffness parameter, which is varied in our simulations. The temperature of the system is kept fixed at 1.0 for all simulations. The mass of each monomer was taken to be 1.0.

In this paper, we have simulated a ring polymer system of 100 rings, each with 100 monomers (total 10000 particles). We randomly packed the ring polymers in a cubic box of length 10^3 (in units of σ) with periodic boundary conditions to create the initial low-density melt configurations. Further, we made sure that the rings remain non-concatenated during packing. The Nosé-Hoover chains thermostat^{56,57} and barostat⁵⁸ were used to control the temperature and the pressure of the system, respectively. We use an overdamped barostat, which couples to the system over a timescale of 1.0. The molecular dynamics simulations were done using LAMMPS⁵⁹.

The pressure on the initial low density melts were iteratively increased for 100 steps with 1000 step intermediate relaxation periods using a time-step of 0.003 until the target pressure is reached. After the compression cycle is completed, the melts were allowed to relax for $\sim 4 \times 10^7$ steps. A total of 10^8 production steps were subsequently ran with a larger time-step of 0.012. This procedure was continued for different state-points from $K_\theta = 1$ to 20, and $P = 0.001$ to 20.0. A few snapshots of the simulation box and an arbitrarily chosen ring polymer at the end of the production

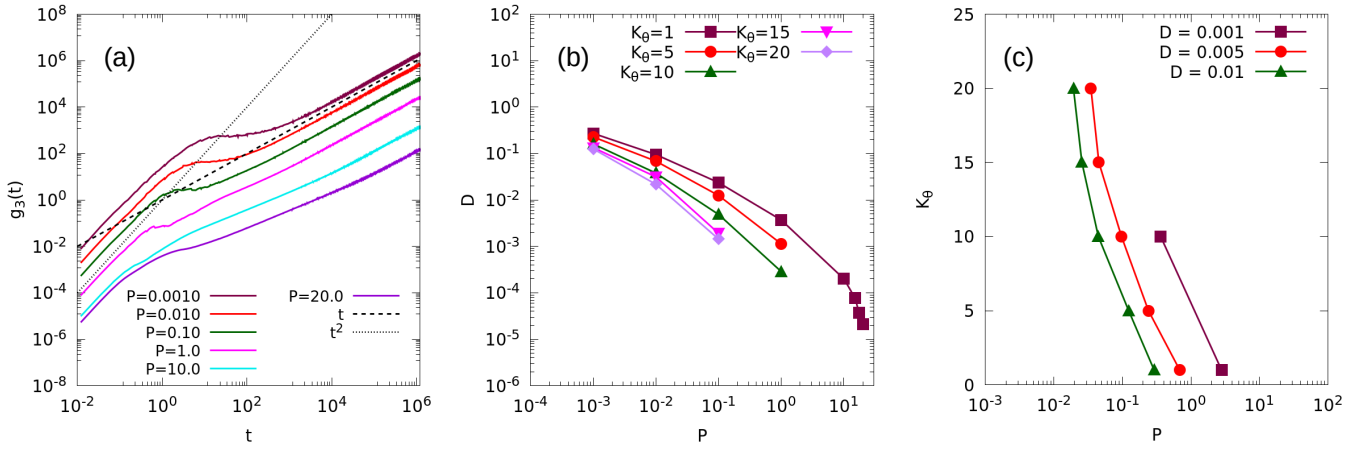


Fig. 2 (a) Variation of the mean square displacement of the center-of-mass of ring polymers ($g_3(t)$) with time, for $K_\theta=1$ and different pressures (P) as marked. Data is only shown for pressure values where equilibrium dynamics is observed within our simulational time window. (b) Center-of-mass diffusion constants (D) calculated from data in (a) are plotted for different values of K_θ as a function of pressure. (c) Estimated isodiffusivity contours, from data shown in (b), for different diffusion constant values, as marked, in $P - K_\theta$ plane.

runs are included in Figure 1.

3 Results

3.1 Equilibrium dynamics

To monitor the dynamical behaviour of the ring polymer melt systems, we study the time evolution of the mean square deviation of the center-of-mass displacement of the ring polymers, $g_3(t)$, which is defined as,

$$g_3(t) = \langle [r_{\text{CM}}(t_0) - r_{\text{CM}}(t_0 + t)]^2 \rangle \quad (4)$$

where t_0 is the reference time origin and $\langle \rangle$ denotes the average over all such time origins and all rings. The corresponding analysis is discussed via Figure 2. For a fixed value of $K_\theta = 1$, the regime in which the ring polymer exhibits a flexible backbone in dilute conditions, the data for $g_3(t)$ is shown in Figure 2(a) for different pressure values. We note that there is variation in the short-time dynamics with changing pressure, even at constant temperature, due to varying box fluctuations resulting from the coupling to a barostat. We have verified that this has no impact on the long-term dynamics.

At late times, we observe diffusive behavior, i.e. $g_3(t) \sim t$. It is evident that this long-time diffusive dynamics shows a slowing down with increasing pressure. This is illustrated via the plot showing the dependence of the extracted center-of-mass diffusion coefficient $D = \lim_{t \rightarrow \infty} g_3(t)/6t$ versus pressure (P) as shown in Figure 2(b), for a range of K_θ values. The data clearly suggests that the onset of slow dynamics depends on both ring polymer stiffness, K_θ , and the pressure: rings with larger K_θ values clearly display eventual onset of glassiness (i.e. $D = 0$ or dynamical arrest) at lower pressures if one extrapolated the D vs P curves. This effect can be seen more clearly in Figure 2(c), where we plot the isodiffusivity lines corresponding to $D = 0.01, 0.005, 0.001$ in the K_θ, P plane. These iso-diffusivity lines drawn within the supercooled regime act as guides to the shape of the eventual line of glass transition in this phase-plane as we vary the stiffness of

the polymers and the ambient pressure.

3.2 Structural Characterization

$K_\theta \backslash P$	0.001	0.01	0.1	1.0
1				
10				
20				Non-equilibrated

Fig. 3 Structures of an arbitrarily chosen ring polymer at various K_θ and pressures are shown in tabular form. All structures shown here belong to the diffusive regime except for $K_\theta=20$ and $P=1.0$, where we could not find a sample of an equilibrated trajectory.

In this section, we characterize the structural variation of the ring polymer melt across the $P-K_\theta$ phase-diagram to understand the possible connection between structure and emergence of slow dynamics. In Figure 4, the variation of average density ($\langle \rho \rangle$), radius of gyration ($\langle R_g \rangle$), and asphericity ($\langle b_s \rangle$) with pressure for different ring polymer stiffness is shown. All data is averaged over all trajectories within a time window of 0.5×10^6 within the equilibrium regime. The structural parameters, R_g and b_s , in three dimensions are defined as⁶⁰,

$$R_g = \sqrt{\lambda_1^2 + \lambda_2^2 + \lambda_3^2} \quad (5)$$

$$b_s = \frac{3 \sum_{i=1}^3 (\lambda_i^2)}{2 \left(\sum_{i=1}^3 \lambda_i \right)^2} - \frac{1}{2} \quad (6)$$

where $\lambda_1, \lambda_2, \lambda_3$ are the principle moments of inertia calculated from the gyration tensor of each polymer. Note that, as defined, low values of b_s correspond to spherical conformations, either crumpled or circular stiff rings and any higher values of b_s suggest more extended structures. Results discussed below, for these two observables, correspond to averages over all rings within configurations sampled in the equilibrium regime.

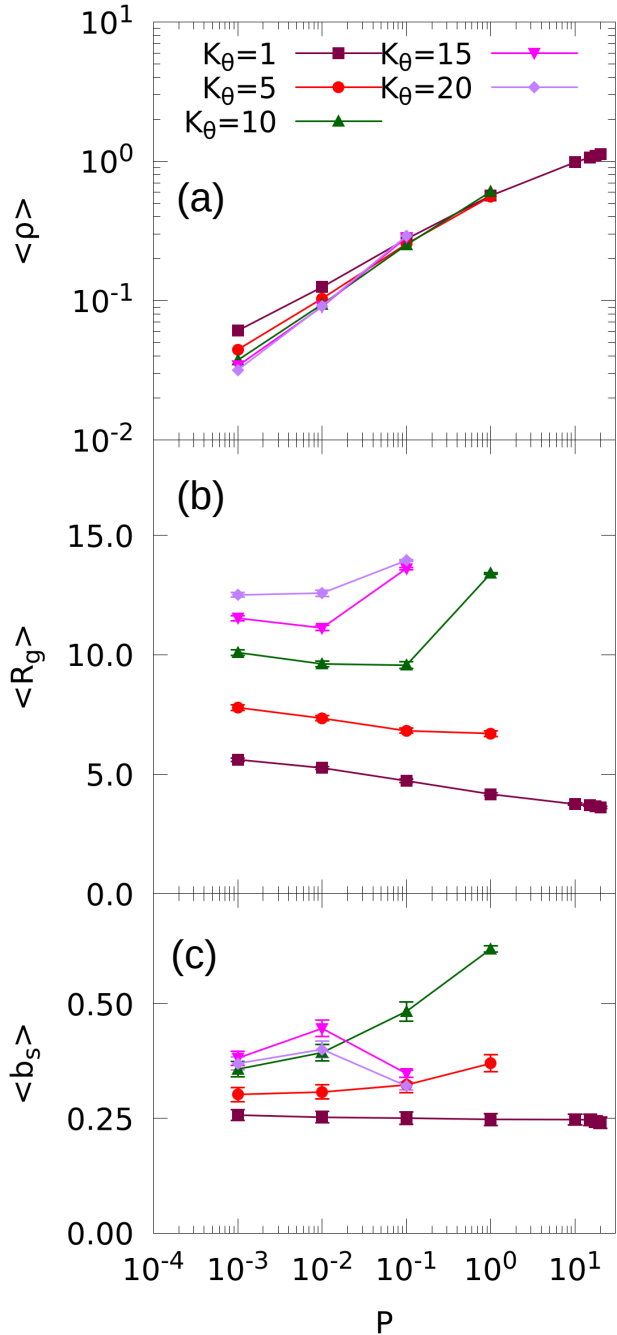


Fig. 4 Average density ($\langle \rho \rangle$), radius of gyration ($\langle R_g \rangle$), and asphericity ($\langle b_s \rangle$) as a function of applied pressure values for different K_θ values, measured under equilibrium conditions.

As can be expected, the average density of the system increases sharply with pressure for all values of K_θ ; see Figure 4(a). How-

ever, it should be noted that the highest values of equilibrium density achieved in our simulations, over the time window of our simulations, is for the most flexible chains (low K_θ). As the chain stiffness increases, the system cannot access high density diffusive regimes, but rather falls out of equilibrium within our observation time window. For example, for the highest and lowest chain stiffness considered in the study ($K_\theta = 20, K_\theta = 1$), the corresponding maximum equilibrium densities achieved are ~ 0.3 and 1.13 , respectively. The $\langle R_g \rangle$ as a function of applied pressure, exhibits varying behavior with different ring polymer stiffness seen in Figure 4(b). For low values of K_θ , with increasing pressure, the value of $\langle R_g \rangle$ monotonically decreases, suggesting a more collapsed conformation adopted by the ring polymers as the density of the system goes up with applied pressure. However, as K_θ values increase, the $\langle R_g \rangle$ values change with applied pressure in a non-monotonic manner. The $\langle R_g \rangle$ values decrease upto a certain pressure, and then increase again, strongly suggesting that the ring polymers might be adopting more extended, plate/rod like structures at higher density. This is further confirmed by the asphericity measurements shown in Figure 4(c), where non-linear behavior of $\langle b_s \rangle$ is found at large K_θ values. For the lowest value of K_θ considered in the study ($K_\theta = 1$), the $\langle b_s \rangle$ values remain invariant with pressure and flexible ring polymers adopt a crumpled conformations at all pressure values, as can be seen in the top row of Figure 3. At the medium values of K_θ considered ($K_\theta = 5, 10$), as pressure increases, the chains tend to adopt more extended structures which is manifested as increase in asphericity values. At higher values of $K_\theta = 15, 20$, as pressure increases, initially there is a slight increase in asphericity values. However, on further increase of pressure, the $\langle b_s \rangle$ values decrease as the rings adopt more spherically stiff plate-like configurations, allowing for better packing of rings as can be seen in the bottom row of Figure 3.

Typically, at a constant temperature, size of the molecules determines the average diffusion coefficient of a system. In case of ring polymers, $\langle R_g \rangle$ values at large K_θ values (≥ 5) seem to have a non-monotonic dependence on pressure, however, the diffusion coefficient does not follow the similar trend (see Figure 2). This behavior suggests that underlying mechanism of the glass formation changes as the system accesses higher P - K_θ state points in the phase diagram. In this region, the polymers adopt more anisotropic extended structures (see Figure 3) compared to the isotropic crumpled-like structures seen at lower values of K_θ . Hence, theories based on diffusion of spherical objects would no longer be applicable in this regime. Here, one has to consider the effect of entanglement to describe the dynamics of the system. The increasing effect of the threading between the ring polymers, a manifestation of entanglement, can describe the dynamical slow-down at higher K_θ values, which we describe in next section.

3.3 Geometric analysis of the threading events

In this section, we correlate the threading of rings and emergence of slow dynamics in ring polymer melts. We develop a threading-detection algorithm, partly based on previously published trian-

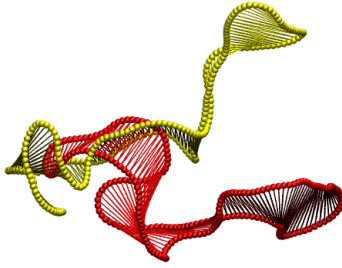


Fig. 5 A pictorial description of a threading event. The horizontal lines inside each ring polymer surfaces depict the minimal surfaces detected by the algorithm.

gulation algorithm³⁰, and incorporating geometric analysis of individual rings. The geometrical analysis was used to identify loops along the contour of the ring polymer which helped to calculate the area of the minimal surface with a higher accuracy as compared to the contour reduction methods³⁰.

To identify threading between any two ring polymers, A and B, we compute all the intersection points between bond vectors of ring polymer A and triangular planes of ring polymer B which lie on the minimal surface of ring polymer B. If number of such intersections points are greater than zero, we assume that A is threaded into B (not the other way around). Due to geometric reasons, total number of intersections will be an even number. The quality of threading is identified by considering the length of the threaded sections^{47,48}. A threading event between ring polymers A and B is defined by the two successive intersections found along the bond vectors of A. The extent of threading, N_{th} is defined as the total number of bond vectors of ring polymer A present between the two successive intersections with ring polymer B. By construction, $N_{th}^{odd} + N_{th}^{even} = N_{ring}$, where N_{th}^{odd} and N_{th}^{even} denote the extent of threading for odd and even threading events, respectively. To quantify the degree of threading, we define a function,

$$\Delta_{th} = 1 - \left| \frac{2 \sum_{i=odd} N_{th}^i}{N_{ring}} - 1 \right| \quad (7)$$

where Δ_{th} is the degree of threading between two ring polymers, who have at least one threading event between them. $\Delta_{th} = 1$ for $\sum_{i=odd} N_{th}^i = N/2$, and $\Delta_{th} = 0$ when $\sum_{i=odd} N_{th}^i = 0$. For a single ring polymer, the mean degree of threading, $\langle \Delta_{th} \rangle$, is determined by averaging over all Δ_{th} with all other ring polymers for all the sampled trajectories. For more details of the threading detection algorithm, see supplementary information, section IA.

3.4 Threading of ring polymers and emergence of spontaneous pinning

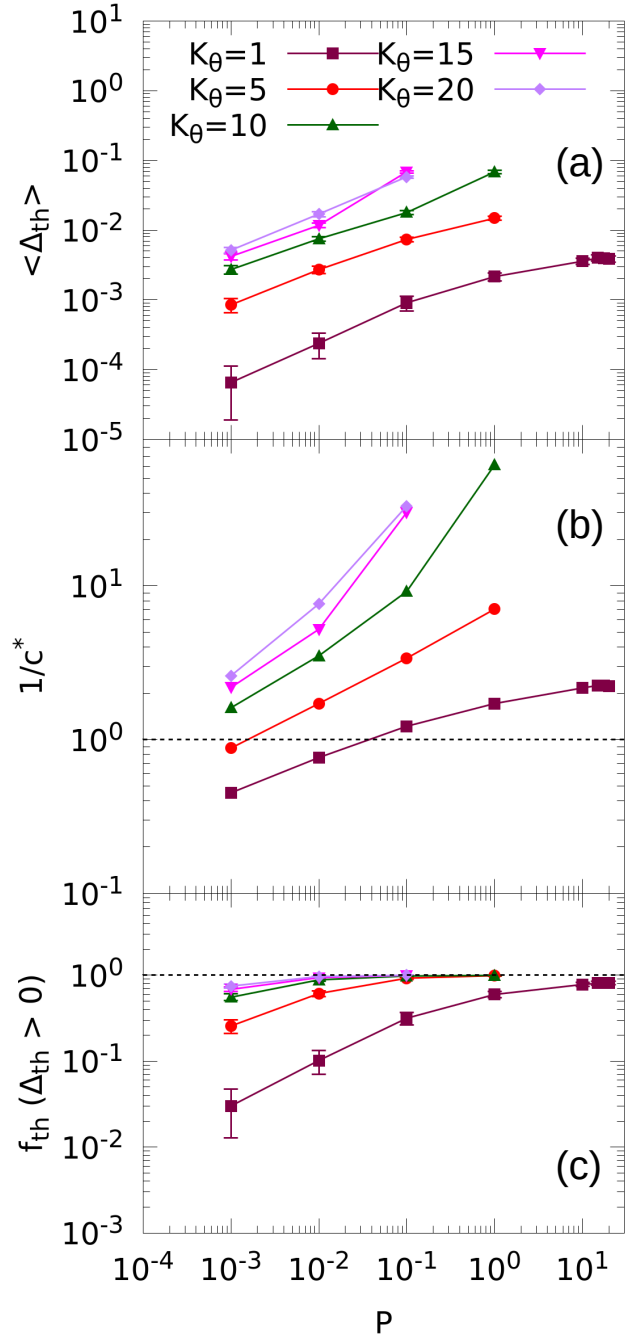


Fig. 6 Variation of (a) average threading factor, (b) inverse of the overlap concentration, and (c) average fraction of threaded rings with different pressure values and ring stiffness, measured within the accessible equilibrium regime. The horizontal dashed line in (b) and (c) cuts the y-axis at 1.

In Figure 6(a), the $\langle \Delta_{th} \rangle$ for the ring polymer melt is plotted as a function of pressure for various values of ring polymer stiffness. For all values of ring polymer stiffness, $\langle \Delta_{th} \rangle$ increases monotonically with pressure suggesting the increase in threading events with the increasing density of the ring polymer melts. While it

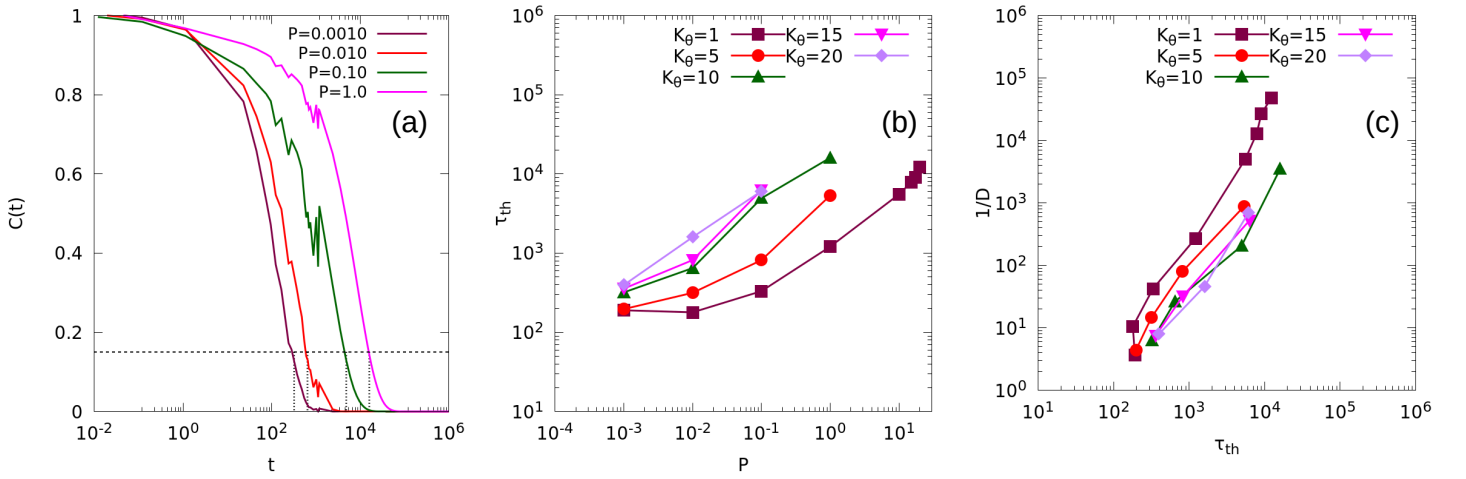


Fig. 7 (a) Variation of $C(t)$ with pressure values at $K_\theta = 10$. A horizontal dashed line is drawn at $C(t) = 0.15$ to obtain the de-threading time scale, τ_{th} . The vertical dashed lines cuts the x -axis at τ_{th} for different pressures. (b) The derived τ_{th} values are plotted against different pressures. (c) Correlation plot between inverse of the diffusion coefficient and τ_{th} for different P - K_θ state points.

is possible to calculate $\langle \Delta_{th} \rangle$ from the simulation trajectories, it is difficult to obtain experimentally⁵¹. On the other hand, $\langle R_g \rangle$, D , and $\langle \rho \rangle$ are readily measurable via experiments. Here, we attempt to find some correlation between the experimentally available structural quantities and $\langle \Delta_{th} \rangle$ calculated from simulations. Any form of entanglement between the ring polymers will result in the polymers overlapping with each other, i.e., the effective size of threaded polymers will be larger than the average volume per ring polymer. Hence, one can define an overlap concentration $c_{R_g}^*$ as,

$$c_{R_g}^* = \frac{3\langle V_m \rangle}{4\pi\langle R_g \rangle^3} \quad (8)$$

where $\langle V_m \rangle = N/\langle \rho \rangle$ is the effective volume per ring polymer and N is the total number of polymers. $c_{R_g}^*$ quantifies the total possible overlap between the hypothetical polymers of size R_g . In Figure 6(a) and 6(b), it can be seen that there is a strong correlation in the trend of $(1/c_{R_g}^*)$ and $\langle \Delta_{th} \rangle$. This correlation suggests that it is possible to estimate the average amount of threading in the ring polymer melt system from the inverse of $c_{R_g}^*$, which can be measured experimentally⁶¹.

However, data in Figure 6(b) shows that the values of $(1/c_{R_g}^*)$ become much larger than 1 with increasing pressure for $K_\theta \geq 5$. Such large increase is possible only if the polymers are highly anisotropic in nature or they form highly entangled conformations. As shown in previous section, anisotropic conformations for high stiff ring polymers were observed in our simulations. Similar emergence of anisotropy in the form of staked-glass phase for ring polymers at high K_θ values has also been seen previously^{62–64}. We predict that in the intermediate K_θ range, it is the entanglement effect which contributes to the increase in $(1/c_{R_g}^*)$ rather than the anisotropy of ring polymers. To verify this, we calculate the change in the average fraction of threaded polymers in the bulk as seen in Figure 6(c). We found that as the bulk system approaches the regime of increasingly slow dynamics, the fraction of threaded rings, f_{th} , sharply increases and saturates to 1. We have

further checked the total fraction of ring polymers which takes part in a high degree of inter-ring threading ($\Delta_{th} > 0.75$, see supplementary information Figure SI.6). Again, we found that the ring polymers prefer a well threaded environment with increasing pressure. Therefore, in the glass phase, we predict that the system must contain a vast network of threaded ring polymers.

The values of $\langle \Delta_{th} \rangle$ respond in a non-monotonic fashion with respect to ring polymer stiffness K_θ at some pressure values (see supplementary information, Figure SI.5), similar to a recent work⁴⁹. This behavior can be attributed to the emergence of hollow disk phase, where rings have lower tendency to thread into each other due to higher stiffness⁴⁹. However, a direct correlation between $\langle \Delta_{th} \rangle$ and diffusion is not straightforward. Some special form of threading between two rings, like square knots, may lead to a slow dynamics despite having a low Δ_{th} value^{52,65}. Hence, the lifetime of a threading event is more important quantity to understand the effect of threading on dynamics of the ring polymers. To understand such temporal evolution of threading event, a threading related correlation function ($C(t)$) for a pair of initially threaded rings is calculated as,

$$C(t) = \frac{\langle \Delta_{th}(t_0)\Delta_{th}(t_0+t) \rangle}{\langle \Delta_{th}^2 \rangle} \quad (9)$$

By definition, $C(t)$ varies from 1 to 0 as the threading correlation decreases between two rings. Once unthreading of the two rings occurs, the threading event no longer exists and therefore the computation of $C(t)$ corresponding to the pair of rings stops. Hence $C(t)$ is similar to a first passage correlator corresponding to an unthreading event between two rings that were initially entangled. In Figure 7(a), we show the variation of $C(t)$ at different pressures with time for a particular stiffness of the ring ($K_\theta = 10$), via which it becomes clear that the decorrelation of the threading event, i.e. unthreading of a pair of threaded polymers, occurs over longer timescales at larger pressures. It is possible to extract a threading lifetime (τ_{th}) by estimating the timescale at which $C(t) = 0.2$. In Figure 6(b), we show the increasing trend of τ_{th}

with pressure, for different K_θ values. Together with Figure 6(b) and Figure 7(b), this result indicates that threading leads to formation of a stable network among the ring polymers, which increases with increasing pressure. It is also evident that for any given pressure, the threading lifetime increases with the stiffness of the ring. A relevant question to ask is how the threading lifetimes can be correlated with the observed dynamical behaviour. In Figure 7(c), we illustrate a positive correlation between τ_{th} and the inverse diffusion coefficient (which would correspond to a diffusive timescale), demonstrating that threading is the most contributing factor for dynamical slowing down with increasing pressure at all K_θ values.

4 Discussion

Emergence of dynamically arrested states in topologically constrained polymer systems is an exciting area which can serve as model platform to explore the dynamics of deformable entities and new phases. Earlier simulations have demonstrated the emergence of glassy dynamics in ring polymers via artificial pinning of the ring polymers, motivated by similar explorations of random pinning in supercooled atomistic liquids⁶⁶. It is not very clear what is the role played by both the ring polymer stiffness and ambient pressure conditions in the formation of such novel phases and whether such an artificial pinning of ring polymers is required for observing the glassy regime.

In this work, we explore the phase space spanned by ring polymer stiffness and ambient pressure to elucidate the emergence of glassy states via large scale simulations of melts of ring polymers formed by 100 monomers. Our simulations show that the tendency towards glassiness emerges without any artificial pinning of the ring polymers for suitable values of ring polymer stiffness. In fact, we demonstrate that stiffer rings are likely to get dynamically arrested at smaller ambient pressures, and correspondingly smaller densities. By calculating various structural properties of ring polymers in the P- K_θ , we show that the ring polymers show a variety of conformations from completely crumpled structures (flexible ring polymers) to elongated and stiff plate like conformations (stiff ring polymers). These structural results strongly suggest that the ring polymers considered here encounter significant dynamical constraints and thus perhaps achieve better close packing via clustering and shape modifications, some of which have been seen earlier^{63,64,67,68,68}. As shown in Figure 3, at low K_θ , the system becomes more closed and globular with increasing pressure. At the medium K_θ range, the rings take a rod like shape at high pressure. At large K_θ , rings take a circular shape which minimizes its energy and helps packing via clustering.

To better understand the emergent slow dynamics with varying ring stiffness and pressure, we explored the possibility of threading among the ring polymers, which has been proposed as a mechanism for the formation of the topological glass that is unique to these objects. For identifying such conformations, a threading algorithm has been developed with specific inputs from the geometry of the ring polymers which gives an excellent quantification of the extent of threading. Our threading analyses strongly suggest that for any specific ring stiffness with increasing pressure values, the average threading factor increases and

contributes to the slow dynamics. Further, the occurrence of such threading events increase with increasing ring stiffness, at any particular ambient pressure condition. We define an experimentally measurable quantity, viz. 'overlap concentration'⁶¹, which strongly correlates with the threading factor measured from simulations. We also measure the life time of a threaded event and find that as the pressure increases, the ring polymers show more long-lived threaded events, in sync with increasing slow down in the dynamics. Taken together all the structural and dynamical properties measured in our simulations, we clearly demonstrate that the emergence of slow, glassy dynamics in ring polymer systems does not require any artificial pinning of the rings. By suitable selection of ring polymer stiffness and pressures applied, slow dynamics can be induced in ring polymers at very low pressure values. We also note that we are observing the formation of such topologically constrained states for relatively smaller ring sizes compared to what has been explored earlier, indicating that the access to such states can be obtained by tuning the properties of the ring.

In future, interesting avenues of study could include the possibility of introducing crowder particles into the ring polymer melt systems or adding differential activities^{65,69-71} to the ring polymer via temperature changes to further probe glass formation in such systems.

Author Contributions

PC and SV conceived the study. PR carried out the simulations. All authors contributed to writing of the manuscript.

Conflicts of interest

There are no conflicts to declare.

Acknowledgments

The authors thank the HPC facility at IMSc, Chennai, for providing the necessary computational platform for this research.

Notes and references

- 1 P. E. Rouse Jr, *The Journal of Chemical Physics*, 1953, **21**, 1272–1280.
- 2 B. H. Zimm, *The journal of chemical physics*, 1956, **24**, 269–278.
- 3 P. De Gennes, *Macromolecules*, 1976, **9**, 587–593.
- 4 R. Zwanzig, *The Journal of Chemical Physics*, 1974, **60**, 2717–2720.
- 5 M. Doi, S. F. Edwards and S. F. Edwards, *The theory of polymer dynamics*, oxford university press, 1988, vol. 73.
- 6 P.-G. de Gennes, *The journal of chemical physics*, 1971, **55**, 572–579.
- 7 M. Doi and S. Edwards, *Journal of the Chemical Society, Faraday Transactions 2: Molecular and Chemical Physics*, 1978, **74**, 560–570.
- 8 R. Granek, *Journal de Physique II*, 1997, **7**, 1761–1788.
- 9 A. Rosa and R. Everaers, *Physical review letters*, 2014, **112**, 118302.

- 10 J. D. Halverson, G. S. Grest, A. Y. Grosberg and K. Kremer, *Physical review letters*, 2012, **108**, 038301.
- 11 J. D. Halverson, W. B. Lee, G. S. Grest, A. Y. Grosberg and K. Kremer, *The Journal of chemical physics*, 2011, **134**, 204904.
- 12 J. D. Halverson, W. B. Lee, G. S. Grest, A. Y. Grosberg and K. Kremer, *The Journal of chemical physics*, 2011, **134**, 204905.
- 13 M. Rubinstein, *Physical review letters*, 1986, **57**, 3023.
- 14 M. Cates and J. Deutsch, *Journal de physique*, 1986, **47**, 2121–2128.
- 15 E. Lee and Y. Jung, *Soft Matter*, 2015, **11**, 6018–6028.
- 16 S. Brown, T. Lenczycki and G. Szamel, *Physical Review E*, 2001, **63**, 052801.
- 17 J. Suzuki, A. Takano, T. Deguchi and Y. Matsushita, *The Journal of chemical physics*, 2009, **131**, 144902.
- 18 E. Lee and Y. Jung, *Polymers*, 2019, **11**, 516.
- 19 T. Deguchi and E. Uehara, *Polymers*, 2017, **9**, 252.
- 20 M. Tark-Dame, R. van Driel and D. W. Heermann, *Journal of cell science*, 2011, **124**, 839–845.
- 21 Y. Zhou, K.-W. Hsiao, K. E. Regan, D. Kong, G. B. McKenna, R. M. Robertson-Anderson and C. M. Schroeder, *Nature communications*, 2019, **10**, 1–10.
- 22 A.-M. Florescu, P. Therizols and A. Rosa, *PLoS Computational Biology*, 2016, **12**, e1004987.
- 23 J. D. Halverson, J. Smrek, K. Kremer and A. Y. Grosberg, *Reports on Progress in Physics*, 2014, **77**, 022601.
- 24 S. Mukhopadhyay and J. Peixinho, *Physical Review E*, 2011, **84**, 011302.
- 25 H. A. Makse, D. L. Johnson and L. M. Schwartz, *Physical review letters*, 2000, **84**, 4160.
- 26 V. M. Batista and M. A. Miller, *Physical review letters*, 2010, **105**, 088305.
- 27 A. Boromand, A. Signoriello, F. Ye, C. S. O'Hern and M. D. Shattuck, *Physical review letters*, 2018, **121**, 248003.
- 28 M. Kapnistos, M. Lang, D. Vlassopoulos, W. Pyckhout-Hintzen, D. Richter, D. Cho, T. Chang and M. Rubinstein, *Nature Materials*, 2008, **7**, 997–1002.
- 29 R. Pasquino, T. C. Vasilakopoulos, Y. C. Jeong, H. Lee, S. Rogers, G. Sakellariou, J. Allgaier, A. Takano, A. R. Brás, T. Chang, S. Gooßen, W. Pyckhout-Hintzen, A. Wischnewski, N. Hadjichristidis, D. Richter, M. Rubinstein and D. Vlassopoulos, *ACS Macro Letters*, 2013, **2**, 874–878.
- 30 D. G. Tsalikis, V. G. Mavrantzas and D. Vlassopoulos, *ACS Macro Letters*, 2016, **5**, 755–760.
- 31 S. P. Obukhov, M. Rubinstein and T. Duke, *Phys. Rev. Lett.*, 1994, **73**, 1263–1266.
- 32 S. P. Obukhov, M. Rubinstein and R. H. Colby, *Macromolecules*, 1994, **27**, 3191–3198.
- 33 A. Y. Grosberg, *Soft Matter*, 2014, **10**, 560–565.
- 34 J. Smrek and A. Y. Grosberg, *Journal of Physics: Condensed Matter*, 2015, **27**, 064117.
- 35 T. Ge, S. Panyukov and M. Rubinstein, *Macromolecules*, 2016, **49**, 708–722.
- 36 D. G. Tsalikis and V. G. Mavrantzas, *ACS Macro Letters*, 2014, **3**, 763–766.
- 37 D. G. Tsalikis, T. Koukoulas, V. G. Mavrantzas, R. Pasquino, D. Vlassopoulos, W. Pyckhout-Hintzen, A. Wischnewski, M. Monkenbusch and D. Richter, *Macromolecules*, 2017, **50**, 2565–2584.
- 38 D. G. Tsalikis and V. G. Mavrantzas, *Macromolecules*, 2020, **53**, 803–820.
- 39 D. G. Tsalikis, T. S. Alexiou, P. V. Alatas and V. G. Mavrantzas, *Macromolecular Theory and Simulations*, 2020, **29**, 2000016.
- 40 Z. E. Dell and K. S. Schweizer, *Soft Matter*, 2018, **14**, 9132–9142.
- 41 D. Michieletto and M. S. Turner, *Proceedings of the National Academy of Sciences*, 2016, **113**, 5195–5200.
- 42 D. Michieletto, N. Nahali and A. Rosa, *Physical Review Letters*, 2017, **119**, 197801.
- 43 D. Michieletto, D. Marenduzzo, E. Orlandini and M. S. Turner, *Polymers*, 2017, **9**, 349.
- 44 D. Michieletto and M. S. Turner, *Physics World*, 2014, 28–30.
- 45 W.-C. Lo and M. S. Turner, *EPL (Europhysics Letters)*, 2013, **102**, 58005.
- 46 E. Lee, S. Kim and Y. Jung, *Macromolecular Rapid Communications*, 2015, **36**, 1115–1121.
- 47 J. Smrek and A. Y. Grosberg, *ACS Macro Letters*, 2016, **5**, 750–754.
- 48 J. Smrek, K. Kremer and A. Rosa, *ACS Macro Letters*, 2019, **8**, 155–160.
- 49 F. Guo, K. Li, J. Wu, L. He and L. Zhang, *Polymers*, 2020, **12**, 2659.
- 50 T. C. O'Connor, T. Ge, M. Rubinstein and G. S. Grest, *Phys. Rev. Lett.*, 2020, **124**, 027801.
- 51 L. R. Gómez, N. A. García and T. Pöschel, *Proceedings of the National Academy of Sciences*, 2020, **117**, 3382–3387.
- 52 B. W. Soh, A. R. Klotz, R. M. Robertson-Anderson and P. S. Doyle, *Phys. Rev. Lett.*, 2019, **123**, 048002.
- 53 K. Kremer and G. S. Grest, *The Journal of Chemical Physics*, 1990, **92**, 5057–5086.
- 54 J. D. Weeks, D. Chandler and H. C. Andersen, *The Journal of Chemical Physics*, 1971, **54**, 5237–5247.
- 55 M. Doi and S. Edwards, *The theory of polymer dynamics*, Oxford University Press, 1988.
- 56 S. Nosé, *The Journal of Chemical Physics*, 1984, **81**, 511–519.
- 57 G. J. Martyna, M. L. Klein and M. Tuckerman, *The Journal of Chemical Physics*, 1992, **97**, 2635–2643.
- 58 S. Nosé and M. Klein, *Molecular Physics*, 1983, **50**, 1055–1076.
- 59 A. P. Thompson, H. M. Aktulga, R. Berger, D. S. Bolintineanu, W. M. Brown, P. S. Crozier, P. J. in 't Veld, A. Kohlmeyer, S. G. Moore, T. D. Nguyen, R. Shan, M. J. Stevens, J. Tranchida, C. Trott and S. J. Plimpton, *Comp. Phys. Comm.*, 2022, **271**, 108171.
- 60 K. Alim and E. Frey, *Phys. Rev. Lett.*, 2007, **99**, 198102.
- 61 W. W. Graessley, *Polymer*, 1980, **21**, 258–262.

- 62 M. Z. Slimani, P. Bacova, M. Bernabei, A. Narros, C. N. Likos and A. J. Moreno, *ACS Macro Letters*, 2014, **3**, 611–616.
- 63 P. Poier, P. Bačová, A. J. Moreno, C. N. Likos and R. Blaak, *Soft Matter*, 2016, **12**, 4805–4820.
- 64 M. Liebetreu and C. N. Likos, *ACS Applied Polymer Materials*, 2020, **2**, 3505–3517.
- 65 I. Chubak, C. N. Likos, K. Kremer and J. Smrek, *Phys. Rev. Research*, 2020, **2**, 043249.
- 66 M. Ozawa, W. Kob, A. Ikeda and K. Miyazaki, *Proceedings of the National Academy of Sciences*, 2015, **112**, 6914–6919.
- 67 M. Bernabei, P. Bacova, A. J. Moreno, A. Narros and C. N. Likos, *Soft Matter*, 2013, **9**, 1287–1300.
- 68 P. Poier, C. N. Likos, A. J. Moreno and R. Blaak, *Macromolecules*, 2015, **48**, 4983–4997.
- 69 J. Smrek, I. Chubak, C. N. Likos and K. Kremer, *Nature Communications*, 2020, **11**, 1–11.
- 70 I. Chubak, S. M. Pachong, K. Kremer, C. N. Likos and J. Smrek, *arXiv*, 2021, **2107.11655**, 1–11.
- 71 D. Vlassopoulos, *Journal Club for Condensed Matter Physics*, 2021, 1–3.